SDSS'Rio 2010 STABILITY AND DUCTILITY OF STEEL STRUCTURES
E. Batista, P. Vellasco, L. de Lima (Eds.)
Rio de Janeiro, Brazil, September 8 - 10, 2010

ADVANCED STABILITY ANALYSIS OF REGULAR STIFFENED PLATES AND COMPLEX PLATED ELEMENTS

László G. Vigh and László Dunai

Budapest University of Technology and Economics, Department of Structural Engineering
e-mail: geri@vbt.bme.hu, ldunai@bme.epito.hu

Keywords: stiffened plate, buckling, imperfection, finite element model, FEM based design.

Abstract
In the paper research on advanced stability analysis of stiffened steel plates are presented. Regular panels are studied by laboratory and virtual tests and the buckling resistances are calculated and evaluated by conventional Eurocode method, by numerical buckling analyses of the plate elements under the actual stress conditions, and by material and geometrical nonlinear finite element analyses imperfections included, following the FEM based design recommendations. The stability analyses of complex plated elements are related to the design of a new Danube tied arch bridge. The non-conventional constructional solutions and complex loading conditions are studied by refined multi-level finite element models. The relative safeties of the different methods of the critical plated elements are determined. The paper highlights the practical problems of the advanced stability analysis: definition of critical point of the element, handling stress concentrations and definition of imperfections.

1 INTRODUCTION

Design methodology based on advanced finite element analysis deserves special attention in the new Eurocodes [1, 2] dealing with buckling analysis of plated structures. The code provides a base in design of special structures with giving the general alternative of using different level of numerical analyses or simulations instead of standardized formulae. In the current research of the authors – partially published in the paper – the design methods of stiffened plates are studied, with a special focus on the application of numerical methods.

In the first phase of the research regular multi-stiffened panels are studied by laboratory tests, with the detailed measurement of the geometric imperfections and residual stresses. In parallel with the experiments the buckling resistances are calculated and evaluated by three different ways: (i) conventional method of the Eurocode 3 for the separate orthotropic plates on the basis of the interaction of the plate and stiffener buckling, (ii) buckling analyses of the plate elements under the actual stress conditions, without separating the cross-section components; the stability resistance is derived on the bases of the critical load factor using the standardized method, and (iii) for model verification purposes, material and geometrical nonlinear finite element analyses with actual imperfections (geometrical imperfections and weld residual stresses) included, i.e. completing virtual experiments.

In the second phase the study is extended for the stability analyses of complex plated elements, related to the design of a new Danube tied arch bridge with a span of 307.8 meters. The non-conventional constructional solutions of the arch and stiffening beam box girders during the erection and the complex loading conditions are studied by refined multi-level finite element models. The relative safeties of the different methods of the critical plated elements in the bridge are determined. The practical problems of the advanced stability analysis raised by the definition of critical point of the element, handling stress concentrations and definition of imperfections are studied.

The experiences on the application of different design methods for practical problems are concluded.

2 USE OF FINITE ELEMENT METHOD IN PLATE STABILITY ANALYSIS

The design and analysis of steel plated structures are specified in Eurocode 3 Part 1-5 (EC3-1-5, [1]). With respect to ultimate limit state analysis, governed by plate stability problems, the following levels can be distinguished (hereinafter called *Method*):

1 basic procedure (no use of numerical models),
2 partial application of numerical models in order to determine plate slenderness,
3 reduced stress method,
4 full numerical simulation.

In *Method 1*, the formulae given in the code are applied, as from the plate slenderness to the reduction factors due to buckling and ultimate capacities inclusive. The reduction factors in any case of stability phenomena are related to the element non-dimensional slenderness parameter $\bar{\lambda}_p$. Generally, it can be written as follows:

$$\bar{\lambda}_p = \sqrt{\frac{F_y}{F_{cr}}} \tag{1}$$

where $\bar{\lambda}_p$ is the non-dimensional slenderness; F_y stands for the ultimate load with no respect to stability problem; while F_{cr} is the critical load corresponding to the stability phenomenon under investigation.

Beside the formulations provided by EC3-1-5 for typical configurations, it is allowed to determine this non-dimensional slenderness by numerical analysis, i.e. through the calculation of critical load. In the above list this is referred as partial application of numerical model (*Method 2*).

The reduced stress method (*Method 3*) is the general version of *Method 2*, where the non-dimensional plate slenderness is determined as:

$$\bar{\lambda}_p = \sqrt{\frac{\alpha_{ult,k}}{\alpha_{cr}}} \tag{2}$$

where $\alpha_{ult,k}$ is the minimum load amplifier for the design loads to reach the characteristic value of the resistance of the most critical point, while α_{cr} is the load amplifier to reach the elastic critical load under complex stress field. Based on this, the reduction factors for each load type (longitudinal, transverse and shear stresses) are to be calculated according to the standard formulae, from which an interpolated value can be determined or, conservatively, the smallest value can be chosen. The outcome of this method is the stress limit for the complex stress field. It can be recognized that this method is in principle the same as the previous one, but works with the general stress field instead of loads. Thus, it can be more generally applied for any complex geometry and stress field. Shortcoming of the method is that limit state is assigned with the most critical point of the structure and thus exceeding the stress limit anywhere means failure of the structure. Additionally, determining the critical point and the governing stability modes could be difficult task.

Ultimate limit checks by non-linear simulation (*Method 4*) are supported by Annex C of EC3-1-5 that provides a general guidance on numerical analysis. It determines the geometrical, material models to be applied. For common structural elements, recommendations on initial (geometric and structural) imperfections are also given. The determined design load amplifier α_u shall cover the design model and analysis uncertainties:

$$\alpha_u \geq \alpha_1 \alpha_2 \tag{3}$$

where α_1 represents the numerical model uncertainties (should be evaluated by test verifications), while α_2 covers the design model uncertainties (γ_{M1} or γ_{M2} partial factors).

Note that EC3 Part 1-6 [2] dealing with shell structures discusses even more general use of FEM.

3 EXPERIMENTAL STUDIES ON MULTI-STIFFENED STEEL PLATE GIRDERS

3.1 Experimental program

To realize the ultimate resistance, an experimental study is conducted on conventionally welded plate girders with multi-stiffened web plate, as shown in Figure 1, [3]. The experimental program is summarized in Table 1. The series included one reference specimen with no stiffener and seven multi-stiffened girders. Flange-to-web joints of girders S8~S12 are prepared by automatic welding, while the longitudinal and vertical stiffeners are placed by manual welding. Except for case J1 where pure bending is obtained by 4-point-loading, the girders are subjected to 3-point-loading arrangement so dominant shear as well as interaction of shear and bending is analyzed. In the design the stiffener dimensions are determined so that overall buckling due to bending is avoided. Failures other than web buckling, namely lateral torsional buckling, flange buckling, etc. are excluded.

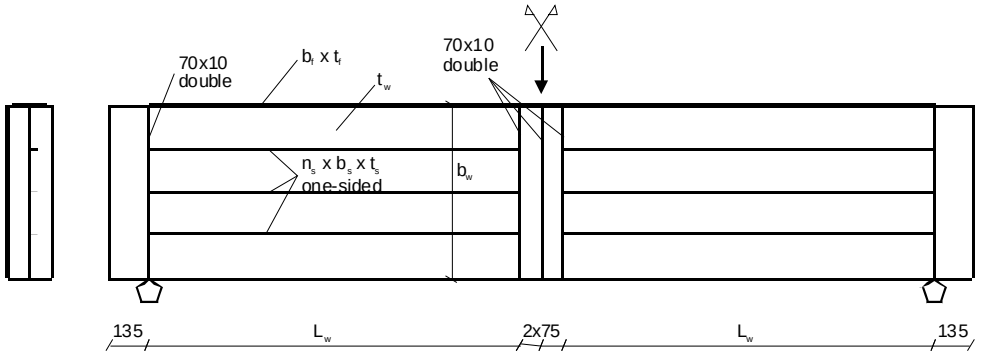

a) 3-point-loading arrangement

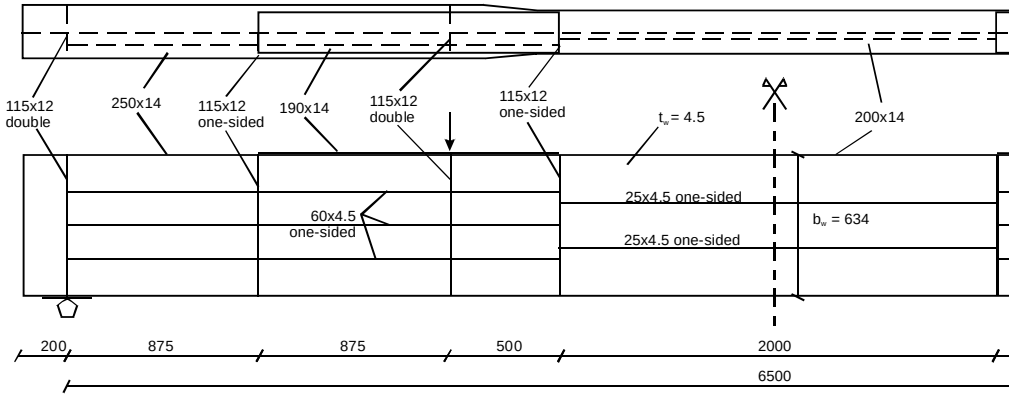

b) J1 girder: 4-point-loading arrangement

Figure 1: Test specimens.

Table 1: Experimental program and results.

Case	L_w [mm]	b_w x t_w [mm]	b_f x t_f [mm]	n_s x b_s x t_s [-, mm]	*Imperfection* [mm] before stiffener production	*Imperfection* [mm] after stiffener production	P_{ult} [kN]	*Failure mode*
S0	1275	600x4	150x (6+6)	---	---	12.7	555	S
S8				3x20x4	8.1	11.2	665	S
S9				3x25x5	12.4	7.2	727	S(+B)
S10				3x30x5	8.4	3.6	729	B(+S)
S12			200x10	3x30x5	4.9	2.1	968	S+B
J1	1902	634x4.5	200x14	2x25x4.5	n.d.	2.5	392	B
J2			260x22		n.d.	4.2	983	S
J3			200x12		n.d.	2.7	629	B(+S)

L_w – web panel length; b_w, t_w – web depth and thickness; b_f, t_f – flange width and thickness;
n_s – number of stiffeners in the web; b_s, t_s – stiffener width and thickness;
n.d. – no data; *S* – shear buckling; *B* – buckling due to bending

3.2 Imperfection measurements

The stiffener production technology has major effect on the occurring imperfection and thus may have large influence on the ultimate behavior.

Geometric imperfections of the entire web plate of each test girder are mapped: with a frequency of 100 mm along the girder length, in each cross-section a continuous measurement is done along the web depth. Measurements before and after the welding of horizontal stiffeners of girders S8~S12 make the evaluation of technology effects available. Table 1 summarizes the results; Figure 2 illustrates the typical imperfection tendency. The stronger stiffener the higher change in shape and magnitude is observed after production. Note that – at this given production technology – the measured imperfections are typically higher than the equivalent geometric imperfection value given in EC3-1-5 (i.e. b_w / 200 = 3 mm). In the extreme case of the un-stiffened web, the actual imperfection is more than four times larger.

Residual stresses caused by welding are also measured by the so-called hole-drilling method. Figure 3 demonstrates the measured residual stresses along the depth of the web. The blue dashed and the continuous lines illustrate the distribution in un-stiffened plate (Dunai et al. [4]) and the stiffened plate [3] welded at the stiffeners, respectively. Well characterized effect of stiffener production can be observed; the difference between the state before and after welding is indicated by the red curve. Between the stiffeners the compressive residual stresses are increased, which is unfavorable with respect to local plate buckling. For further details on imperfection measurements and analysis of different welding technologies refer to [3, 4].

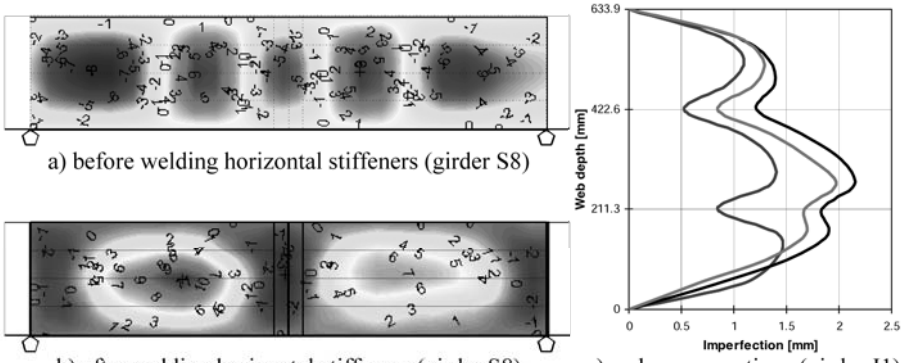

a) before welding horizontal stiffeners (girder S8)

b) after welding horizontal stiffeners (girder S8)

c) web cross-sections (girder J1)

Figure 2: Typical geometric imperfections.

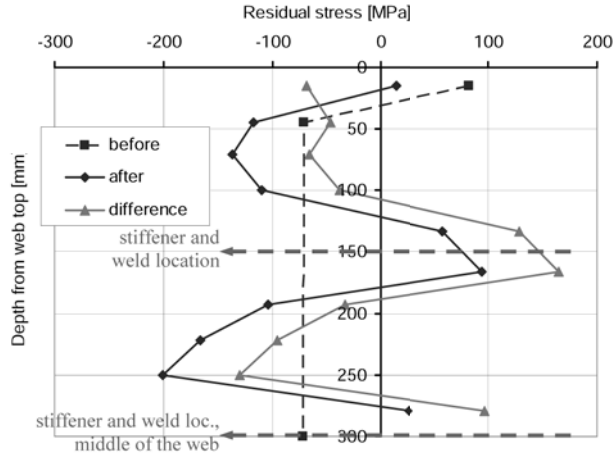

Figure 3: Residual stress distributions before and after welding of horizontal stiffeners.

3.3 Ultimate capacity

Figure 4 shows the obtained load-deflections diagrams of the tested eight girders, while typical failure modes are illustrated in Figure 5.

The results confirm the efficiency of small stiffeners in shear and bending capacity, thus the applicability of the conceived configuration. By increasing the stiffener size the ultimate capacity is efficiently improved, accompanying by a gradual change of failure mode of shear buckling to plate buckling due to bending. Negligible increase in the capacity value can be observed between S9 and S10 girders. This means that, from structural point of view, the optimal stiffener size is 25x5 mm for this girder geometry and loading: i.e. overall buckling due to bending is excluded and shear capacity reaches the bending resistance. For further discussion of the test results refer to [3].

The test results are used for numerical model verifications, and are qualitatively as well as quantitatively compared to the theoretical, numerical and standard results, discussed in the following sections.

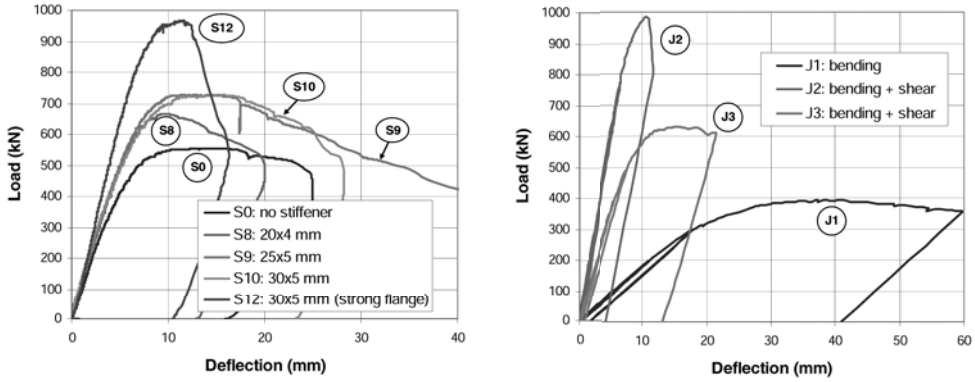

a) experiments 'S' b) experiments 'J'

Figure 4: Experimental load-deflection diagrams.

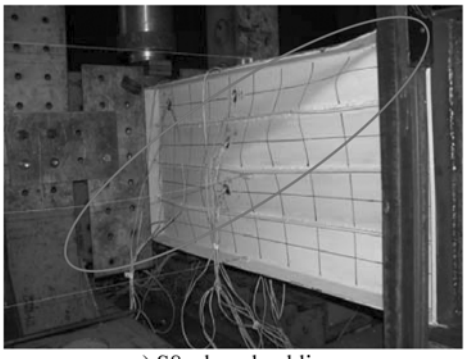

a) S8: shear buckling

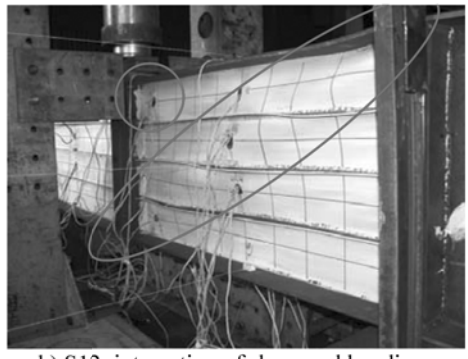

b) S12: interaction of shear and bending

Figure 5: Typical experimental failure modes.

4 STABILITY RESISTANCE CALCULATION FOR TEST GIRDERS

4.1 Standard Eurocode calculation

According to EC3-1-5, multi-stiffened (orthotropic) plates subjected to compression, bending and shear have to be analyzed with respect to the following failure modes:

- local plate buckling between stiffeners and plate buckling of stiffeners due to direct stresses,
- overall plate buckling due to axial stresses, plate-type behavior,
- overall plate buckling due to axial stresses, column-like behavior,
- overall and local plate buckling due to shear.

The local plate buckling is considered by the application of cross-section classification and effective width. For the overall buckling, the non-dimensional slenderness for plate-type and column-type behavior has to be separately determined, as follows:

$$\bar{\lambda}_p = \sqrt{\frac{\beta_{A,c} f_y}{\sigma_{cr,p}}}\ ,\ \bar{\lambda}_c = \sqrt{\frac{\beta_{A,c} f_y}{\sigma_{cr,c}}} \tag{4, 5}$$

where $\bar{\lambda}_p$ and $\bar{\lambda}_c$ are the slendernesses for plate- and column-type behavior; $\sigma_{cr,p}$ and $\sigma_{cr,c}$ are the corresponding critical stresses; f_y is the yield stress. $\beta_{A,c}$ reflects the reduction in effective area due to local plate buckling. For plate-type behavior the plate buckling reduction factors (ρ) shall be then applied, while the column-like buckling is represented by the column buckling curves (reduction factor χ_c). The following interaction formula is applied to find the reduction factor ρ_c:

$$\rho_c = (\rho - \chi_c)\xi(2-\xi) + \chi_c \text{, where } \xi = \frac{\sigma_{cr,p}}{\sigma_{cr,c}} - 1, \quad but\ 0 \le \xi \le 1 \tag{6, 7}$$

This reduction factor shall be applied for the compression parts of the plate except for the strips near-side the plate edges. The method is illustrated in Figure 6.

Shear buckling resistance is calculated on the basis of plate slenderness obtained from the elastic buckling stress. According to EC3-1-5 the stiffener effect is considered via an additional buckling coefficient term $k_{\tau,st}$.

$$k_\tau^{(ov)} = \begin{cases} 4.00 + \dfrac{5.34}{\alpha^2} + k_{st} & \alpha < 1 \\ 5.34 + \dfrac{4.00}{\alpha^2} + k_{st} & \alpha \geq 1 \end{cases} \tag{8}$$

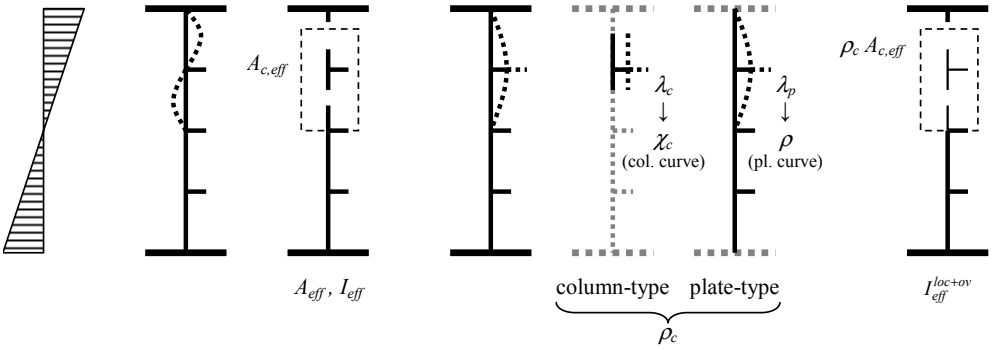

a) local buckling b) overall buckling c) overall + local buckling

Figure 6: Stiffened plate girder subjected to bending – EC3-1-5 method.

4.2 Buckling coefficients of multi-stiffened plates

In the framework of parametric study invoking energy method, elastic buckling of plates stiffened with multiple stiffeners is analyzed in [3, 5]. Based on the results, buckling coefficients are formulated. Interaction of the different loads, as well as overall and local buckling is also investigated.

The author proposed modifications for the standard Eurocode calculations of critical loads in [3, 5]. On the one hand, the modifications aim to generalize the buckling coefficient formula for interaction of compression and bending. On the other hand, corrections of shear buckling coefficient is made to increase the accuracy and to consider interaction of local and overall shear buckling where relevant [3].

Note that the theoretical achievements and the conceived concept are also verified by numerical and experimental studies [3].

4.3 Calculation of tested girders with Methods 1 and 2

For the tested girders, ultimate capacities are calculated according to EC3-1-5. In the calculation, the λ_w plate slenderness for shear is determined either by the original formulas provided by EC3-1-5 (denoted as *orig.*) or by the help of the modified buckling coefficient formulas proposed by the authors (*mod.*). The plate slenderness λ_p for bending is calculated only by the proposed modifications. Actual material properties are applied; the yield stress of the web plate at specimens S0~S12: f_y^{web} = 479 MPa, at girders J1~J3: f_y^{web} = 380 MPa.

Completing the calculation, it is found that overall buckling is characterized by plate-type behavior (ξ = 1), and that – except for girder S8 – the reduction factor ρ_c = 1, meaning that overall buckling is not dominant. Consequently, the standard calculation also reflects that these small stiffeners efficiently impede the overall buckling due to bending. Comparing the standard results to the test values (Table 2), it is clear that the original EC3-1-5 procedure underestimates the shear resistance: the difference varies between -30% and -6%.

Application of the modified critical stress formulations (practically meaning *Method 2*) leads to better approximation of the shear resistance, as Table 2 and Figure 7 confirm. The difference between the original and the modified procedure is larger in case of three stiffeners (S8~S12), while it can be neglected in case of two stiffeners (J2~J3). Note that the deviation increases with stronger stiffener. It is

also an important observation that the modified calculation gives the actual failure back: while the standard method indicates interaction failure for girder S10, the modified one results in bending failure that actually occurred in the test.

The accuracy of the formulas regarding overall plate buckling due to bending cannot be in general evaluated by the tested girders as this failure mode is mostly excluded. Further verification is carried out by the help of extended virtual experiments, as discussed in [3].

Table 2: Ultimate resistance of the tested girders – Comparison.

Case	λ_p [-]	λ_w [-] orig.	λ_w [-] mod.	P_{Rd} [kN]	P^*_{Rd}, P_{ult} [kN] orig.	mod.	FEM	test
S0	1.31	2.48		394	457		569	555
S8	1.01	1.99	1.83	479	544	577	677	665
S9	0.87	1.85	1.57	506	575	642	691	727
S10	0.83	1.72	1.38	531	604	667	718	729
S12				595	684	840	993	968
J1		---		234	339		411	392
J2	0.84	1.71	1.66	564	733	752	972	983
J3				464	587	598	631	629

λ_p – non-dimensional plate slenderness for direct stresses; λ_w – non-dimensional plate slenderness for shear stresses; P_{Rd} – design resistance according to EC3-1-5; P^*_{Rd} – resistance based on actual material properties; *orig.* – standard method; *mod.* – modified standard method; *FEM* – virtual experiments

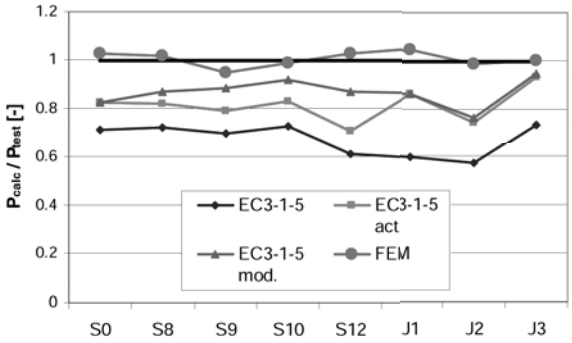

Figure 7: Comparison of the results.

4.3 Model development and verification – Virtual experimenting

For the further investigations, advanced finite element model is developed and numerical studies are carried out by the authors. Simultaneously to the real tests, virtual experiments – that is defined as full non-linear simulation representing the actual conditions (real imperfections, material, etc.) – are also executed. The virtual experimenting of the actual real tests on the steel girders supported the development and verification of the numerical model. In the second phase, additional parametric study – not detailed here – on the effect of different fabrication processes are also conducted by extended virtual experiments using the verified model [3].

The numerical analyses are completed by the ANSYS [6] finite element program system. In the numerical model, 4-node quadrilateral shell elements (designated as SHELL 181 in ANSYS) are applied (Figure 8), with a maximum side length of 20-50 mm, aligning to the residual stress shape.

Material and geometrical non-linearity is taken into account. Actual stress-strain relations of the steel material are set for the material non-linear behavior. The von Mises yield criterion is applied.

Initial stresses caused by welding are considered in the models (Figure 2). The involved stress-distribution type represents the conventional manufacturing method: the usual values of 60% and 30% of the yield stress are applied to the tensile (at weld position, i.e. at the stiffeners) and compressive stresses, respectively. Geometrical imperfections are derived from the actual measurements discussed above.

In the analyses large displacements are considered. Displacement-controlled calculations are completed, i.e. loading is represented by gradually increasing displacements, better reflecting the experimental conditions. The analysis proceeds up to a certain set limit of displacement.

The iteration is completed on the bases of Newton-Raphson method. The convergence of the iterations is checked by the Euclidian norm of the unbalanced forces and moments; the applied convergence tolerance factor is 0.1%.

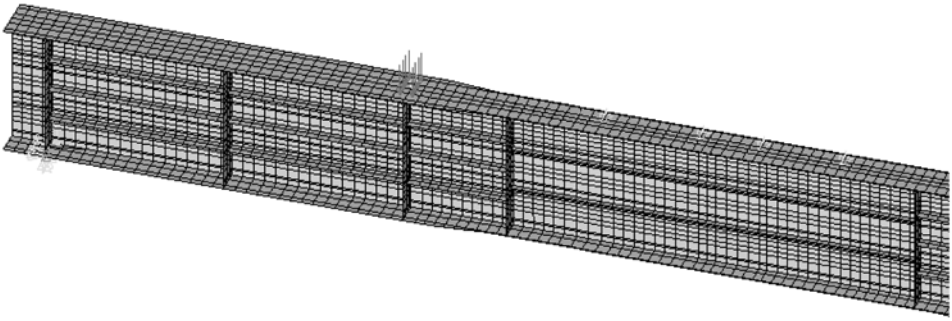

Figure 8: Finite element model of multi-stiffened plate girders.

Figure 9 shows the load-deflection curves obtained from the real as well as the virtual tests. The figure confirms that the simulation is in high accordance with the actual tests with respect to the overall behavior. As it is observed, the shape of the load-deflections curves coincide and the ultimate load capacities are close to the test results, which are also compared in Table 2 and Figure 7. The difference in ultimate loads is less than 5% in every case.

Comparison of failure modes similarly concludes that the model is reliable: the virtual experiment leads to the same failure as observed in the tests. An illustration is given in Figure 10.

As a consequence, the developed model well reflects the actual complex behavior of the multi-stiffened plate girders, thus it is applicable in further studies and design, too. By numerical simulation or virtual experimenting all the relevant details can be considered, and as the results prove, advanced numerical simulation may be rewarding due to the increased resistance.

Note that application of realistic imperfections has major importance in achieving accurate simulation, as the deformed shape may differ when the initial imperfection has different shape and magnitude from the actual one (e.g. as proposed by EC3-1-5, using buckling shape as imperfection, which may force one failure mode to dominate instead of occurring interaction modes). The imperfection sensitivity with these respects has not been studied yet; this task is involved in a separate research by Jakab et al. [7].

4.4 Effects of fabrication process

The research published in [3] involved further parametric studies on the effect of different fabrication processes, by extended virtual experiments using the verified numerical model. The analysis is extended to aluminum girders as well. Influence of different assumed initial imperfections resulted by different fabrication processes (e.g. MIG or FSW welding) and configurations is investigated. Based on the results, general conclusions are drawn on the applicability of the conceived configurations. Comparing to results obtained by the EC3-1-5 and EC9-1-1 standards, the standardized methods are also evaluated, and corrections are proposed.

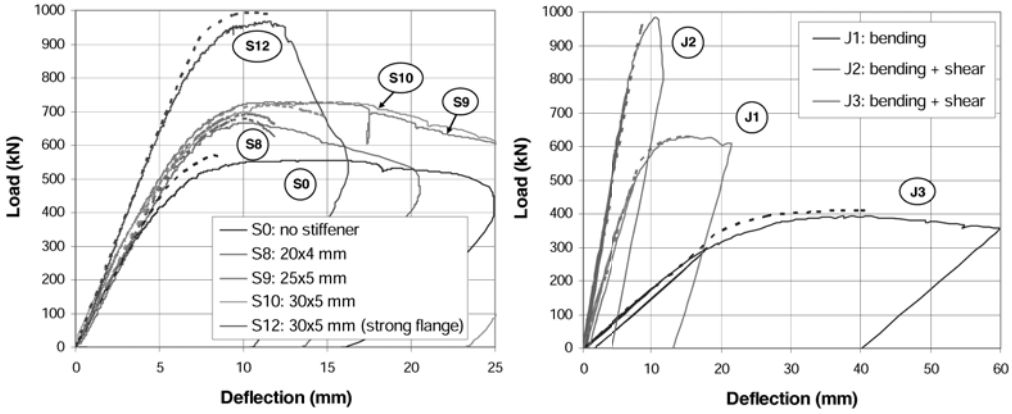

Figure 9: Comparison of test and FEM results – Load-deflection curves.

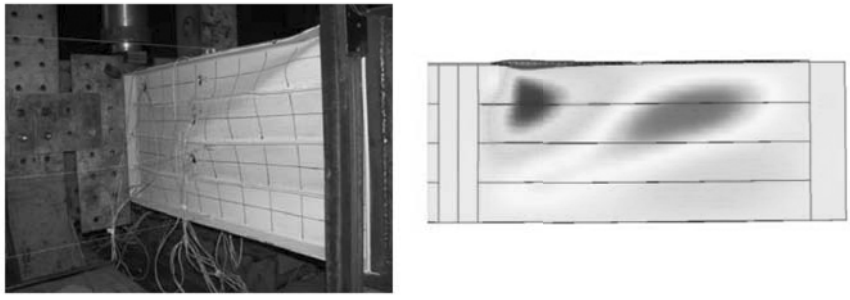

a) S8: shear buckling

b) S12: interaction of shear and bending

Figure 10: Comparison of test and FEM results – Failure modes.

5 COMPLEX STIFFENED PLATE ELEMENTS OF A NEW DANUBE BRIDGE

A new Danube bridge is recently erected in Hungary: its main span is a basket handle shaped tied arch bridge, with a length of 307.8 m (Horváth et al. [8]). The height of the circular shaped arches is 48 m; the inside dimensions of the arch box cross-sections are 1960*3720 mm; the stiffening beams are parallelogram shaped box sections, with 2100 mm wide flanges and 3100 mm inner height. The walls of the arch and stiffening beam box sections are stiffened by open (flat and T-shape rib) longitudinal stiffeners; the thickness of the box sections varies from 20 to 50 mm.

The main bridge is assembled on a platform at the river bank and shipped to the final position. During the shipping operation, temporary supporting bars are installed near to the supports, to strengthen the structure over the barges. Figure 11 shows the erection of the bridge.

Figure 11: Erection of the arch bridge.

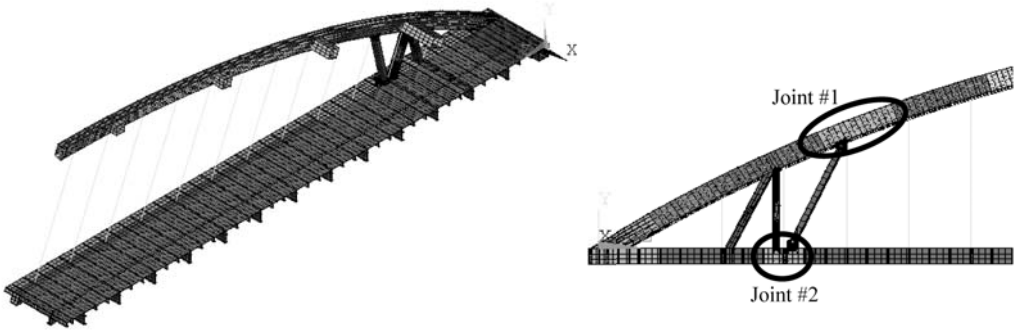

Figure 12: Global shell finite element model.

Global shell finite element model is developed for the investigation of the erection process, assuming double symmetry of the geometry, boundary conditions and loadings, as shown in Figure 12.

Six sub-models are developed in [9] to study in details the critical joints, owing refined meshes; their boundaries conform to the global model, from which the compatible displacements as the sub-model loads are derived. The structural details and the results of the stability analyses of two complex joints, marked in Figure 12, are illustrated in the following sections of the paper.

The plate elements in the joints are classified according to the shapes and the stress field, as follows:

1. dominantly compressed stiffened plates (Joint #1, Figure 13),
2. stiffened plate subject to complex stress field (Joint #2, Figure 14/a),
3. irregular configuration and stress field (Joint #2, Figure 14/b,c).

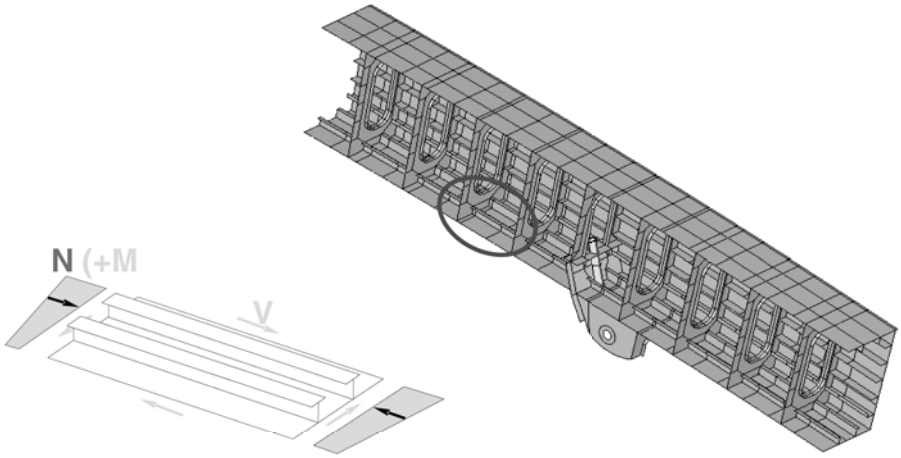

Figure 13: Longitudinally stiffened plate element in arch and supporting bar Joint #1.

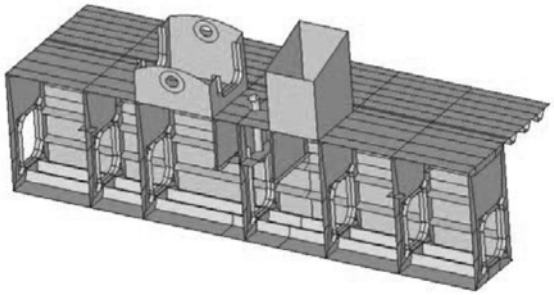

a) Joint #2

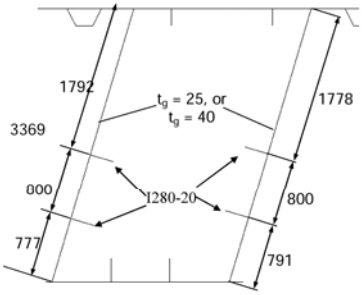

b) stiffened web configuration

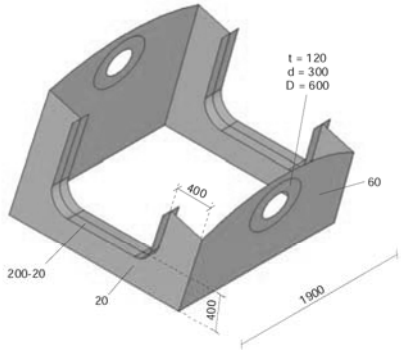

c) gusset plates of pinned connection

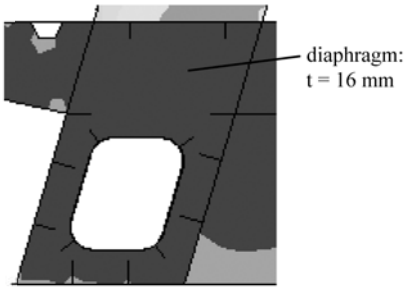

d) typical diaphragm

Figure 14: Plate elements in stiffening beam and supporting bar Joint #2.

6 STABILITY ANALYSES AND RESULTS

6.1 Longitudinally stiffened plates under compression

Beside the standard checks according to the relevant Hungarian codes, six of the critical stiffened panels subjected to pure compression are selected for detailed, advanced checking. Table 3 lists the geometry data of the investigated configurations; the yield stress of the material is f_y = 460 MPa.

Table 3. Investigated configurations and results of standard Method 1.

Case Nr.	t_p [mm]	b [m]	a [m]	stiffener	χ_c [-]	ρ [-]	ξ [-]	ρ_c [-]	ϕ [-]	ϕf_y [N/mm^2]
1	40	2	4.56	2 x 280-22	0.532	1.000	0.676	0.951	0.945	435
2	30	3.8	4.56	5 x 280-22	0.587	0.896	0.000	0.587	0.619	285
3	50	2	2.125	2 x T270-150-22	0.915	1.000	0.000	0.915	0.938	432
4	20	3.8	3.9	5 x 280-22	0.721	1.000	0.000	0.721	0.676	311
5	16	3.8	3.86	5 x 280-22	0.761	1.000	0.000	0.761	0.637	293
6	20	2	3.86	2 x 280-22	0.723	1.000	0.000	0.723	0.698	321

t_p – plate thickness; b – plate width; a – plate length between transverse stiffeners or diaphragms

6.1.1 Standard method (Method 1)

In accordance to EC3-1-5, resistance is calculated on the basis of effective cross-section calculation. For comparison reasons, the general reduction factor ϕ is introduced, standing for the ratio of the effective and gross area. Table 3 shows the obtained results. It can be observed that – except for the first case – column-like behavior is dominant ($\xi = 0$).

6.1.2 Method 2 and 3

In case of pure compression, *Method 2* (use of linear stability analysis) and *Method 3* (reduced stress method) lead to the same results. According to the method, critical stresses of the stiffened plate have to be evaluated by numerical analysis: bifurcation analysis is completed on FE models developed by ANSYS program. Three adjacent panels are modeled by shell elements as shown in Figure 15. Both the overall and local buckling shapes are determined. Typical buckling shapes are shown in Figure 16. The obtained overall buckling modes confirm that the plates are relatively short, which is also found by the standard analysis. As stated, overall buckling precedes local buckling in all the cases.

In Table 4, the calculated critical stresses for overall buckling are compared to the EC results. It is observed that the buckling stress formula given in EC3 1-5 is in good accordance with the FE calculations in case of compression. This also means that *Methods 1 and 2* do not lead to significant deviations in the ultimate load.

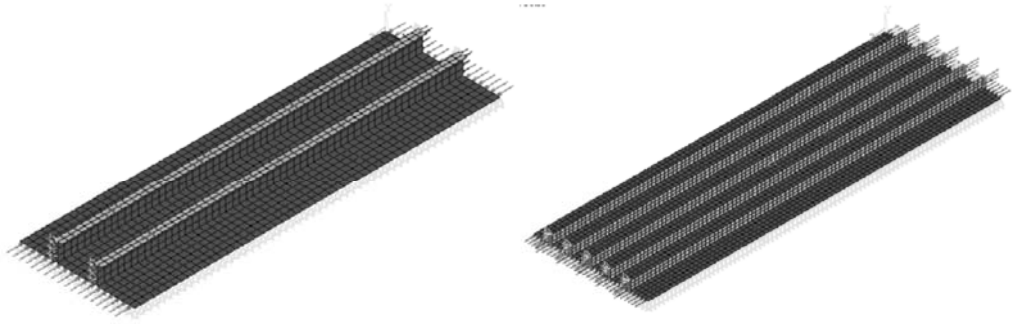

Figure 15: Numerical models of two typical stiffened panels.

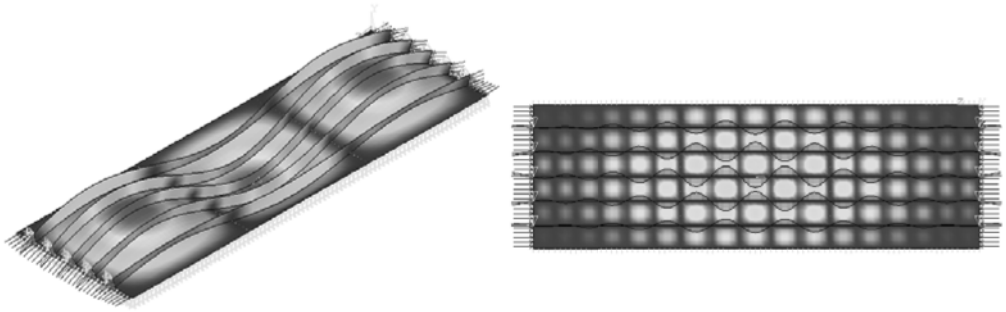

a) overall plate buckling b) local plate buckling

Figure 16: Plate buckling modes from linear stability analysis.

Table 4. Critical stresses for overall buckling.

Case	Critical stress [N/mm^2]		diff.
Nr.	EC3-1-5	FEM	[%]
1	868	931	7.3
2	578	588	1.7
3	3598	3560	-1.1
4	902	881	-2.3
5	995	955	-4.0
6	865	969	12.0

Table 5. Comparison of Methods 1 and 4.

Case	Ultimate load [N/mm^2]		diff.
Nr.	Method 1	Method 4	[%]
1	435	448	3.0
2	285	314	10.2
3	432	452	4.6
4	311	365	17.4
5	293	370	26.3
6	321	404	25.9

6.1.3 Non-linear simulation (Method 4)

The non-linear simulation is completed using the same geometrical model. Standardized material models and imperfections are applied. Figure 17 illustrates the material model: linearly elastic - perfectly plastic – with a fictive hardening to overcome numerical instability. The imperfections to be applied in the analysis are distinguished by the code with respect to the failure mode under investigation. In the studied case:

- "global" imperfection of longitudinal stiffener (Figure 17/a), with a magnitude of $e_{0w} = \min(a/400, b/400)$,
- local imperfection of plate panels or sub-panels (Figure 17/b), with a magnitude of $e_{0w} = \min(a/400, b/400)$,
- local imperfection of stiffener subject to twist (Figure 17/c), with a magnitude of $\phi_0 = 1/50$.

Generally, these imperfections should be combined, choosing a leading imperfection with full magnitude and the additional imperfections can be considered with magnitudes reduced to 70%. As in the studied case the local plate buckling between stiffeners is not dominant, its imperfection can be neglected. The overall buckling shapes typically includes the other two imperfections, thus, the buckling shapes may be applied as imperfections; however, it complicates the adaptation of the 70%-rule, since the magnitudes of the different imperfections included are linearly coupled. As reference, the magnitude is chosen as the global imperfection value satisfies the criterion. If the twist imperfection is considered as leading, the global imperfection becomes extremely large in certain cases. Note that the standard allows the usage of corresponding buckling shapes as imperfections in any case.

In the completed study the α_2 factor – representing the design model uncertainties equals to 1.0. The numerical model is verified by real experiments as discussed earlier. Based on the verification, the α_1 factor – representing the numerical model's uncertainties – also equals to 1.0.

Figure 18 shows the load-deflection curves of typical cases. Ultimate capacity calculated by EC3-1-5 and results corresponding to large imperfection (i.e. choosing the twist imperfection as leading) are also indicated. As the figure confirms, the extremely large imperfection may lead to large differences in certain cases.

6.1.4 Comparison

As it is already stated, *Method 1 and 2* do not give significant differences because of the concurrent critical stresses. Hereafter, just *Method 1 and 4* are compared.

Table 5 lists the calculated ultimate loads. It can be observed that the difference between the standard method and full numerical analysis can exceed 25%. Note that as it is also found by [3], the differences can be even higher if actual strain hardening is also taken into account. It is observed that with increasing dominance of buckling the underestimation by the standard method (compared to FEM) is also increasing, thus, the larger the slenderness, the larger the safety. Needless to say, when failure occurs due to overall yielding, there is no difference in the results (Case 1 and 3).

However, the authors should emphasize that the imperfections proposed by EC3-1-5 are dependent only on the plate dimensions *a* and *b*, and independent from the fabrication process, stiffener geometry, etc., which would otherwise significantly influence the actual imperfections. In this way, it is queried whether the proposed imperfection magnitude is sufficient or not. Consequently, the conclusion of the above comparison can be drawn in two ways:

1 If the applied imperfections are assumed sufficient, the safety in the standard EC method can be relatively large.
2 If the applied imperfections are not sufficient, the FE analysis cannot be considered accurate, and the arising error is on the unsafe side.

Recall that the measurements discussed in Section 3 presume larger amplitude of imperfections than the ones currently applied in the code. Note that the analyses are completed with 2-4 times larger imperfections (leading twist imperfections) as well. Even with this extreme imperfection, the analyses – except for Case 2, where anyway overall yielding is dominant – give larger load capacity than *Method 1*.

It is also noted that with increasing slenderness the imperfection sensitivity is also increasing.

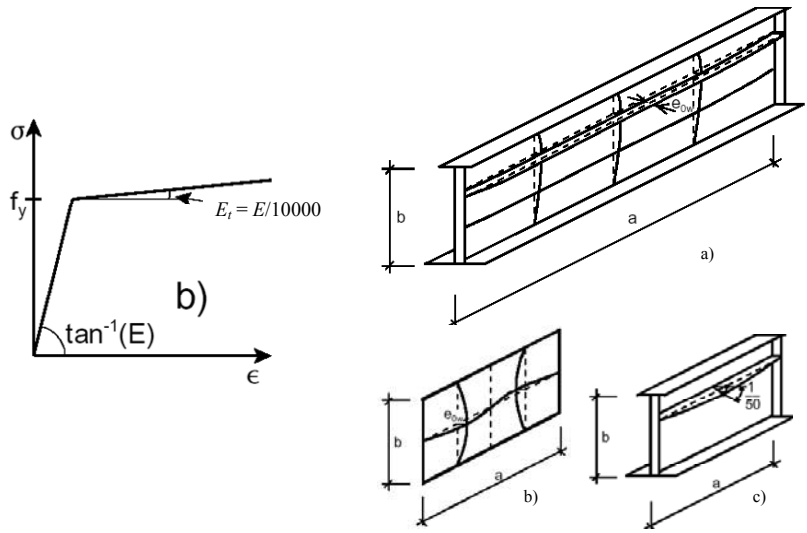

Figure 17: Applied material model and equivalent geometrical imperfections.

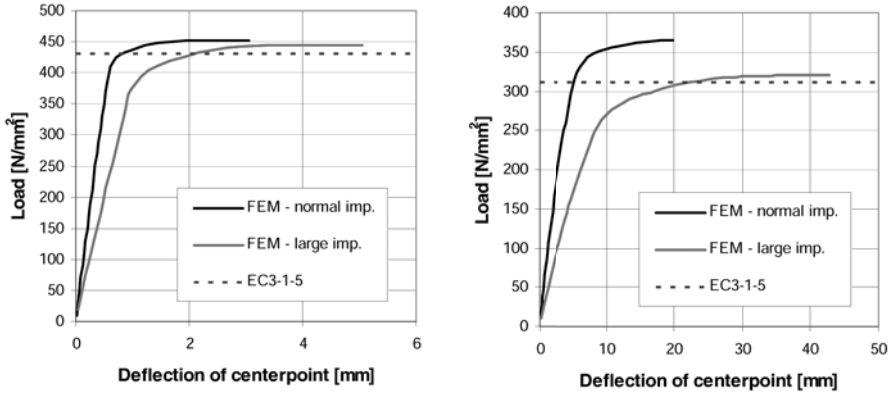

a) Case #3 b) Case #4

Figure 18: Typical results of the non-linear simulation.

6.2 Complex plated elements

In the following sections, application of the reduced stress method is illustrated on complex plated elements subjected to complex stress field. Strength and stability check of more than a hundred of details is completed by the help of the shell-element sub-models mentioned in Section 5 [9]. Analysis of three representative details is briefly summarized hereafter.

Due to the complex stress field and/or the complex geometry, these details can hardly be handled by the basic standard method. In absence of prescribed equivalent geometrical imperfections, the use of *Method 4* is not practical either. As a reasonable alternative, the reduced stress method (*Method 3*) is applied, even though – as it is discussed in the following sections – it may be laborious and troublesome, too. The general outline of *Method 3* is tabulated in Table 6. Through the discussion of the representative examples, special attention is paid to the following aspects and problematic points that practically may arise:

- modeling of the plated element,
- definition of the critical point of the element and the strength load amplifier,
- determination of governing failure mode and choice of buckling reduction curve.

The shell-element sub-models allow accurate stress and linear stability analysis of the stiffened plated members, considering the complex interaction behavior of the adjacent elements.

6.2.1 Stiffened plates subject to complex stress field

During the erection of the bridge, simultaneous action of bending, shear and direct transverse loading applies in the longitudinally stiffened web plate in the vicinity of the temporary bars (Figure 14/a,b), causing the complex stress field shown in Figure 19. In this case, definition of the critical point of the element is relatively straightforward. Figure 20/a shows the buckling shape of the panel under investigation; the corresponding critical load amplifier: α_{cr} = 6.99. The high value presumes that the element is not sensitive for buckling. Details of the calculation are given in Table 7.

Crucial point is the determination of the buckling reduction factor. The reduction factors related to the different failure modes (i.e. direct stresses, shear, etc.) are determined on the basis of the general slenderness parameter. Due to the complex stress field, various buckling curves are to be used even for this single case (Figure 21) and the choice is not straightforward. For simplification, Annex B of EC3-1-5 provides a general plate buckling curve (also indicated in Figure 21) that gives conservative, but

reasonable approximations for the different load cases. Additional difficulty is that regarding the longitudinal and transverse buckling modes, one has to analyze the possibility of column-like or plate-type post-critical behavior. Equations 6 and 7 shall be used for the interpolation between the two behavior types. For this, determination of the column critical load amplifier $\alpha_{cr,c}$ (or $\sigma_{cr,c}$) would require a numerical model in which the corresponding longitudinal edges are relieved from adjacent elements. Following this rule would highly complicate the analysis, losing the benefits of such advanced modeling. Alternatively, it can be conservatively assumed that column-like buckling occurs.

Table 6: Outline of Method 3.

Step	Description		
1	strength load amplifier	$\alpha_{ult,k} = f_y / \sigma_{red}$ from linear elastic analysis	(9)
2	critical load amplifier	α_{cr} from linear elastic buckling analysis	
3	slenderness parameter	$\bar{\lambda}_p = \sqrt{\frac{\alpha_{ult,k}}{\alpha_{cr}}}$	(10)
4	buckling reduction factor	a) conservative approach: $\rho = \min(\rho_x, \rho_y, \chi_w)$ or	(11)
		b) interpolated values of ρ_x, ρ_y, χ_w	(12)
5	resistance check	$\frac{\rho \alpha_{ult,k}}{\gamma_{M1}} \geq 1.0$	(13)

σ_{red} – acting Von-Mises stress; $\alpha_{ult,k}$ – load amplifier to reach first yield; α_{cr} – load amplifier to reach elastic critical load; γ_{M1} – partial factor; ρ_x, ρ_y and χ_w are corresponding buckling reduction factors for longitudinal, transverse and shear stresses, respectively, taking into account column-like behavior if relevant

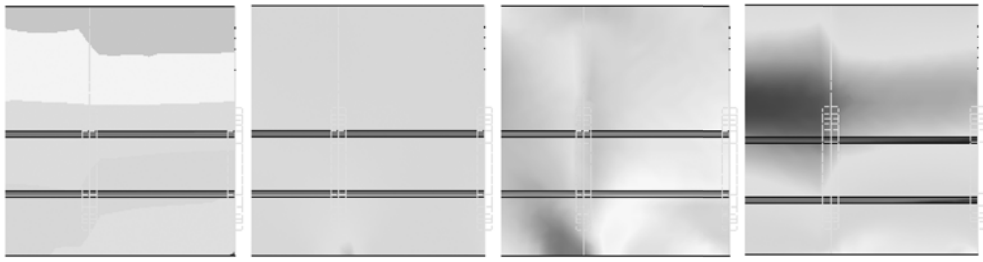

$\sigma_{x,max}$ = 214 MPa | $\sigma_{y,max}$ = 90 MPa | τ_{max} = 29 MPa | $\sigma_{red,max}$ = 187 MPa

a) longitudinal | b) transverse | c) shear | d) Von-Mises

Figure 19: Stress components – Multi-stiffened web.

Table 7: Complex details – Results of Method 3.

Case	Description	σ_{red} [MPa]	$\alpha_{ult,k}$ [-]	α_{cr} [-]	λ_p [-]	ρ [-]	type of curve used	$\frac{\rho \alpha_{ult,k}}{\gamma_{M1}}$
1	web – load introduction	187	1.90	6.99	0.521	0.83	column	**1.58**
2	diaphragm	68	5.22	7.12	0.856	0.84	gen. plate	**4.38**
		316	1.12	7.57	0.385	0.91	column	**1.02**
3	pinned connection	100	3.55	7.57	0.685	0.73	column	**2.59**
		355	1.00	7.57	0.363	0.92	column	**0.92**

σ_{red} – acting Von-Mises stress; λ_p – non-dimensional general plate slenderness; ρ – general reduction factor; $\alpha_{ult,k}$ – load amplifier to reach first yield; α_{cr} – load amplifier to reach elastic critical load

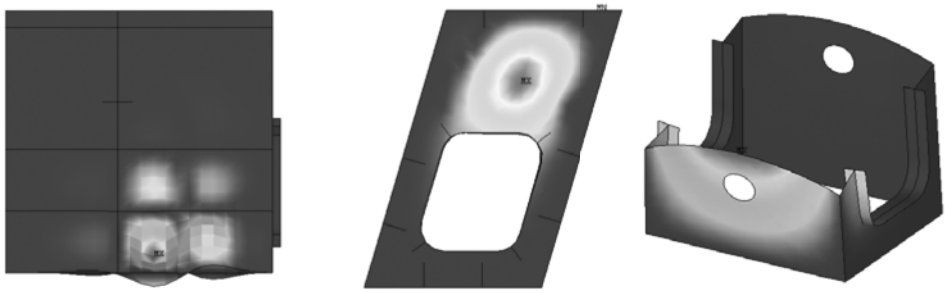

α_{cr} = 6.99 α_{cr} = 7.12 α_{cr} = 7.57

a) multi-stiffened web b) diaphragm c) gusset plate stiffening bar

Figure 20: Plate elements in stiffening beam and supporting bar Joint #2 – Buckling shapes.

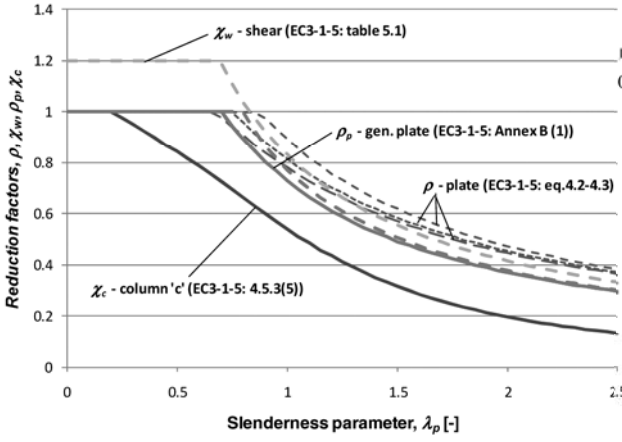

Figure 21: Different buckling curves (reduction factors).

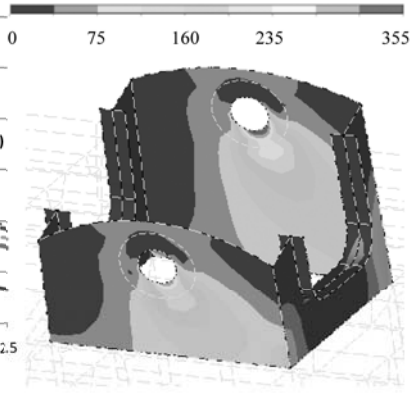

Figure 22: Von-Mises stress distribution in the gusset plates

6.2.2 Diaphragm

For the case of the typical 16-mm-thick diaphragm (Figure 14/d), critical stress for column-like buckling is easy to predict: it is certainly less than 20 MPa regarding any direction. Thus, it can be stated that plate-type behavior governs the failure (Figure 20/b shows the buckling mode). Table 7 lists the corresponding results.

6.2.3 Complex geometry elements – Gusset plate of pinned connection

The gusset plate of the pinned connection (Figure 14/c) is complex in terms of geometry as well as stress distribution (Figure 22). Definition of critical point of the element is complicated and as Table 7 confirms it may drastically change the outcomes with respect to strength as well as failure mode (how slender the element is). Rigorously taking the words of the code would mean one has to consider the peak stress arising in the vicinity of pin hole that reaches the yield stress. This would result in unsatisfactory element. However, this local plasticization does not characterize the overall behavior. Selecting more representative stress values leads to reasonable and satisfactory results (the uniform stress of 100 MPa reflects uniform bearing stress distribution).

Determination of buckling reduction factor is also complicated by the fact that a type of distortional stability failure mode occurs with interaction of the gusset plate and the stiffening diaphragms (Figure 20/c). Conservatively, column buckling mode is considered; however, selecting more reasonable plate buckling curves would drastically change the results: for the relevant slenderness parameter one may find yielding instead of stability failure (i.e. reduction factor equals to 1.0).

6.2.4 Shortcomings of the advanced methods

As demonstrated, the general use of the *reduced stress method* for complex plated elements is complicated by the facts that:

1) Definition of critical point of the element is not straightforward:
   a) Finite element analysis may result in unrealistic peak stresses due to the mesh.
   b) Element stability behavior is not necessarily related to the peak stress (e.g. bearing stress distribution along perimeter of pin hole).
   c) The analysis does not necessarily reflect whether a certain buckling mode governs the failure.
2) Choice of appropriate buckling curve is not straightforward:
   a) High confidence is needed to estimate the actual failure mode and post-critical behavior.
   b) To combine plate-type and column-like behavior, one may have to analyze the same detail with different boundary conditions, which is not practical, especially when the element boundaries cannot be clearly defined.
3) The method may lead to extremely conservative results and thus uneconomic design, which may set back its use:
   a) The limit state is assigned with the most critical point of the structure and thus exceeding the stress limit anywhere means failure of the structure.
   b) Accordingly, conservatively selecting the worst cases (i.e. peak stress point and column buckling curve) may result in extremely underestimated capacity of the whole element or may presume certain failure (e.g. eligibility of the pinned connection cannot be confirmed).

The above problems could be overcome by using *full non-linear simulation* or virtual experimenting. However, such simulation requires careful detail modeling, relatively accurate estimations on material behavior and imperfections.

7 CONCLUSIONS

In the paper the stiffened plates are studied by experimental, standard based and advanced stability analyses. The investigations are related to regular test plate elements and complex plated elements of a bridge. The conclusions of the research can be drawn on different fields, as follows:

Buckling checking of regular stiffened plates:

- Based on experimental, numerical and theoretical studies buckling coefficients are of multi-stiffened plates are formulated and modifications are proposed for the standard Eurocode calculations of critical loads.
- The application of the modified critical stress formulations leads to better approximation of the shear resistance and it gives back the experimentally observed actual failure mode.

FEM based buckling checking:

- Geometrically and material nonlinear FE models are developed in parallel with experiments considering measured geometrical imperfections and residual stresses.
- The results of the analyses are in high accordance with the actual tests with respect to the ultimate behavior and capacities.
- By the virtual experimenting all the relevant details can be considered, and the results prove that FEM based design using advanced numerical simulation may be rewarding due to the increased resistance.

Practical checking of irregular plates by FEM analysis:

- Different plate buckling design methods are applied to check the complex plate elements on a new Danube bridge in Hungary, under dominant compression stress, subjected to complex stress field and having irregular configuration and stress field.
- By comparison of the results it is concluded the difference between the standard method of the Eurocode and full numerical analysis can exceed 25% for dominantly compressed multi-stiffened elements.
- Practical shortcomings of using the reduced stress method of Eurocode standard for complex geometry and stress field on the basis of numerical calculation are observed due to the (i) uncertainties of definition the critical point of the element, (ii) choice of appropriate buckling curve.

The advanced stability analysis is refined for stiffened plates and extended for other type of structures (e.g. girders with trapezoidally corrugated webs) in the frame of ongoing research of the authors.

ACKNOWLEDGEMENT

The presented research is conducted under the partial financial support of the OTKA T049305 project of the Hungarian National Science Foundation.

REFERENCES

[1] *EN 1993-1-5:2005 Eurocode 3 – Design of steel structures – Part 1-5: Plated structural elements*, Final Draft, CEN, Brussels, 2005.

[2] *EN 1993-1-6:2005 Eurocode 3 – Design of steel structures – Part 1-6: Strength and stability of shell structures*, CEN, Brussels, 2005.

[3] Vigh, L.G., *Virtual and real test based analysis and design of non-conventional thin-walled metal structures*, PhD dissertation, Budapest University of Technology and Economics, 2006.

[4] Dunai, L., Jakab, G., Néző, J., Topping, B.H.V., "Experiments on welded plate girders: fabrication, imperfection and behaviour", *Proc. 1st International Conference on Advances in Experimental Structural Engineering (AESE '05)*, Vol. 1, pp. 51-58, Nagoya, Japan, 19-21 July, 2005.

[5] Vigh, L.G., "On the Eurocode buckling formulas of multi-stiffened metal plates", *Proc. of International Colloquium on Stability and Ductility of Steel Structures (SDSS 2006)*, Vol. 1, pp. 545-552, Lisbon, Portugal, 6-8 September, 2006.

[6] *ANSYS Structural Analysis Guide*, Online Documentation ANSYS Inc., 2005.

[7] Jakab, G., Szabó, G., Dunai, L., "Imperfection sensitivity of welded beams: experiment and simulation", *International Conference in Metal Structures: Steel – A New and Traditional Material For Building (ICMS 2006)*, pp. 173-182, Brasov, Romania, 20-22 September, 2006.

[8] Horváth, A., Dunai, L., Domanovszky, S., Pesti, Gy., "The Pentele Danube bridge in Dunaújváros, Hungary; design, research and construction", *Bauingenieur*, pp. 419-438, 2008.

[9] Dunai, L., Farkas, Gy., Szatmári, I., Joó, A., Tóth, A., Vigh, L.G., *Dunaújváros Danube Bridge – River Bridge – Additional static analyses 2* (in Hungarian), 7th research report, BME Department of Structural Engineering, Budapest, August 2006.